Nuclear Medicine and Biology 93 (2021) 54–62

Contents lists available at ScienceDirect

Nuclear Medicine and Biology

journal homepage: www.elsevier.com/locate/nucmedbio

Radiolabelling and positron emission tomography imaging of a high-affinity peptide binder to collagen type 1

Maria Rosestedt [a], Irina Velikyan [a], Ulrika Rosenström [a], Sergio Estrada [a], Ola Åberg [a], Jan Weis [b], Christer Westerlund [c], Sofie Ingvast [d], Olle Korsgren [d], Patrik Nordeman [a], Olof Eriksson [a,c,*]

[a] Science for Life Laboratory, Department of Medicinal Chemistry, Uppsala University, Uppsala, Sweden
[b] Department of Medical Physics, Uppsala University Hospital, Uppsala, Sweden
[c] Antaros Medical AB, Mölndal, Sweden
[d] Department of Immunology, Genetics and Pathology, Uppsala University, Uppsala, Sweden

ARTICLE INFO

Article history:
Received 2 July 2020
Received in revised form 23 October 2020
Accepted 22 November 2020

Keywords:
Positron emission tomography
Collage type 1
Fibrosis
NASH
NAFLD

ABSTRACT

Introduction: Pathological formation of fibrosis, is an important feature in many diseases. Fibrosis in liver and pancreas has been associated to metabolic disease including type 1 and 2 diabetes. The current methods for detecting and diagnosing fibrosis are either invasive, or their sensitivity to detect fibrosis in early stage is limited. Therefore, it is crucial to develop non-invasive methods to detect, stage and study the molecular processes that drive the pathology of liver fibrosis. The peptide LRELHLNNN was previously identified as a selective binder to collagen type I with an affinity of 170 nM. Radiolabelled LRELHLNNN thus constitute a potential PET tracer for fibrosis.
Method: LRELHLNNN was conjugated to a DOTA/NOTA moiety via a PEG_2-linker. DOTA-PEG_2-LRELHLNNN was labelled with Gallium-68 and NOTA- PEG_2-LRELHLNNN with aluminium fluoride-18. Biodistribution of [^{68}Ga]Ga-DOTA-PEG_2-LRELHLNNN and [^{18}F]AlF-NOTA-PEG_2-LRELHLNNN was performed in healthy rats ex vivo and in vivo. The ^{68}Ga-labelled analogue was evaluated in a mouse model of liver fibrosis by PET/MRI-imaging. The human predicted dosimetry of the tracers was extrapolated from rat ex vivo biodistribution studies at 10, 20, 40, 60, 120, 180 min (only fluoride-18) post-injection.
Results: The peptides were successfully radiolabelled with gallium-68 and aluminium fluoride-18, respectively. The biodistribution of [^{68}Ga]Ga-DOTA-PEG_2-LRELHLNNN and [^{18}F]AlF-NOTA-PEG_2-LRELHLNNN was favorable showing rapid clearance and low background binding in organs where fibrosis may develop. Binding of [^{68}Ga]Ga-DOTA-PEG_2-LRELHLNNN to fibrotic liver was higher than surrounding tissues in mice with induced hepatic fibrosis. However, the binding was in the range of SUV 0.3, indicating limited targeting of the tracer to liver. The extrapolated human predicted dosimetric profiles of [^{68}Ga]Ga-DOTA-PEG_2-LRELHLNNN and [^{18}F]AlF-NOTA-PEG_2-LRELHLNNN were beneficial, potentially allowing at least three PET examinations annually.
Conclusions: We describe the modification, radiolabelling and evaluation of the collagen type I binding peptide LRELHLNNN. The resulting radiotracer analogues demonstrated suitable biodistribution and dosimetry. [^{68}Ga]Ga-DOTA-PEG_2-LRELHLNNN exhibited binding to hepatic fibrotic lesions and is a promising tool for PET imaging of fibrosis.
Advances in knowledge: Validation of a new collagen targeting PET tracer.
Implications for patient care: Early, non-invasive diagnosis and stratification of fibrosis in order to improve the diagnosis, staging and treatment of patients with diseases involving fibrosis.

1. Introduction

The definition of fibrosis is the formation of connective tissues that might occur as a response to injury, which is known as scarring. However, excess formation and deposition of connective tissue, which constitutes the pathological formation of fibrosis, is an important feature in many different diseases affecting, e.g. lung, heart, kidney and liver [1].

Liver fibrosis has been associated to metabolic disease and type 2 diabetes (T2D). Non-alcoholic fatty liver disease (NAFLD) and non-alcoholic steatohepatitis (NASH) involves chronic inflammation triggering the activation of fibroblasts which in turn leads to production and deposition of extracellular matrix such as collagen. As the early development of hepatic fibrosis is rather asymptomatic and painless, the time until NASH diagnosis may be delayed, and the risk of progression to severe conditions such as liver cirrhosis might occur [2,3].

* Corresponding author at: Department of Medicinal Chemistry, Uppsala University, Dag Hammarskjölds väg 14C, 3tr, SE-751 83 Uppsala, Sweden.
E-mail address: olof.eriksson@ilk.uu.se (O. Eriksson).

https://doi.org/10.1016/j.nucmedbio.2020.11.006

Today, the treatment and monitoring of hepatic fibrosis is hampered by the lack of suitable methods for detecting and diagnosing the disease. The current methods such as fine needle aspiration biopsy is invasive, with risk of injury and sampling errors, and there is a lack of plasma biomarkers that could be used to diagnose and detect the changes in the fibrosis development as response to interventions [4].

Therefore, it is of crucial importance to develop non-invasive methods in order to detect, diagnose, stage and study the molecular processes that drive the pathology of fibrosis. This would potentially contribute to an early stage identification of the disease and enable assessment of treatment effect.

Collagen type I is a key component of fibrosis formation. Thus, targeting of collage type I by molecular imaging could potentially provide a direct and quantitative assessment of the stage of fibrosis. The peptide LRELHLNNN with high affinity to collagen type I was recently reported based on the collagen binding residues of the decorin protein [5,6] (Fig. 1A). The LRELHLNNN affinity towards collagen type I was $K_d = 170$ nM, which is approximately 10 times higher than for the previously described imaging probes targeting collagen type I, e.g. CBP8 [4,7–9] and collagelin [10–14].

Here, we describe the modification of the LRELHLNNN peptide with two different chelators and the subsequent labelling using the positron emission tomography (PET) radionuclides gallium-68 and fluoride-18. Furthermore, the resulting constructs [^{68}Ga]Ga-DOTA-PEG$_2$-LRELHLNNN (Fig. 1B) and [^{18}F]AlF-NOTA-PEG$_2$-LRELHLNNN (Fig. 1C) were evaluated preclinically for the binding to liver fibrosis.

2. Material and methods

2.1. Animals and materials

All animals were kept in ventilated cages, with food and water supply and a 12 h day/night cycle. All animals were treated according to the European Union rules on animal care and were approved by the animal ethics committee in Uppsala, Sweden (permit number: 5.8.18-06578/2019).

The purchased chemicals were used without further purification: amino acids (Novabiochem, Switzerland, Sigma-Aldrich, Sweden, Iris Biotech GmbH, Germany), PyBOP (Novabiochem, Switzerland), 2CTCresin (Iris Biotech GmbH, Germany), Fmoc-O2Oc-OH (Iris Biotech GmbH, Germany), DOTA(tBu)$_3$-OH and NOTA(tBu)$_2$-OH (CheMatech,

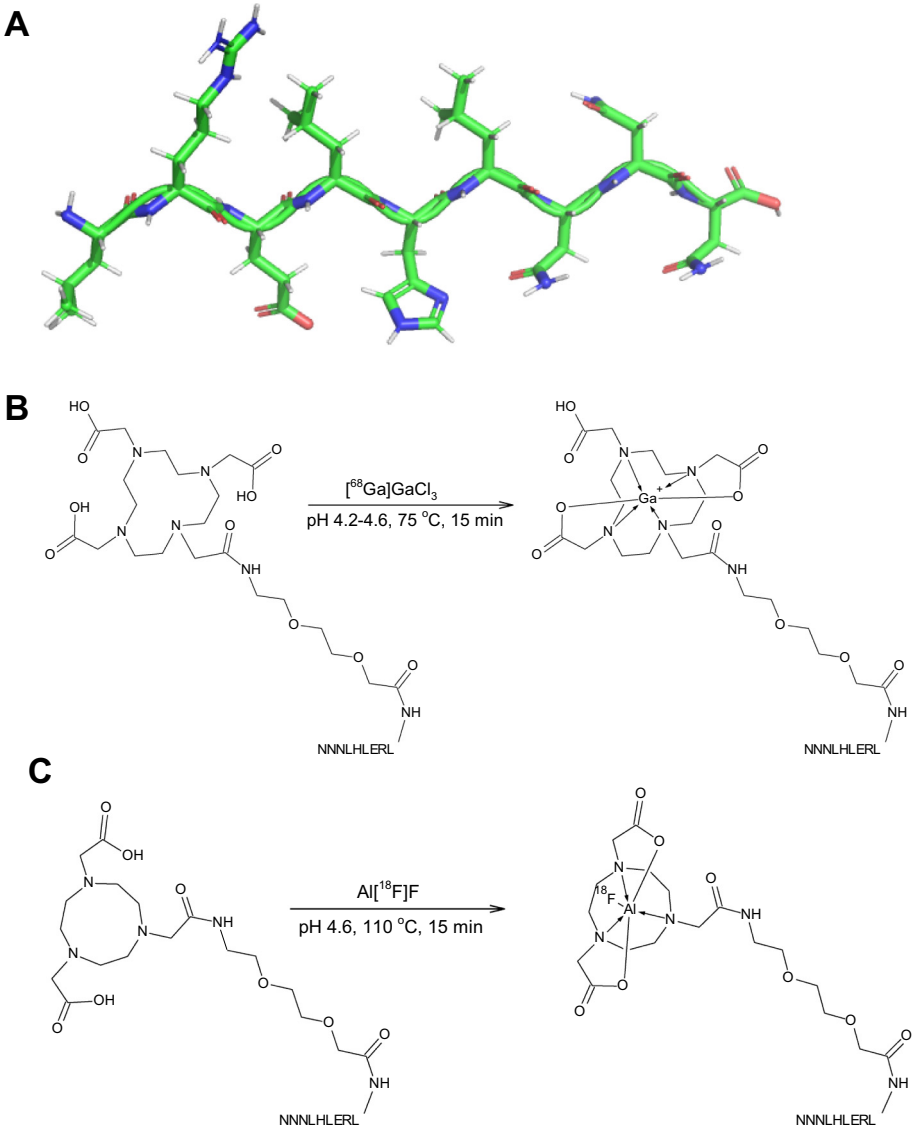

Fig. 1. Molecular structure of the unconjugated LRELHLNNN peptide (A). Schematic presentation of labelling reactions: labelling of DOTA-comprising analogue with [68Ga]Ga (B); labelling of NOTA-comprising analogue with Al[18F]F (C).

France), piperidine (Sigma-Aldrich, Sweden), DMF (Fisher Scientific, UK), sodium acetate buffer (pH 4.6, 31048, Sigma-Aldrich, Stockholm, Sweden), 30% HCl (Ultrapure, 1.00318.0250 Merck, Sigma-Aldrich) and trifluoroacetic acid (TFA, Merck, Darmstadt, Germany).

2.2. Peptide synthesis and radiochemistry

Standard solid-phase peptide synthesis (SPPS) was used to synthesis the precursor peptides by conjugating 2-(4,7,10-tris(2-(*tert*-butoxy)-2-oxoethyl)-1,4,7,10-tetraazacyclododecan-1-yl)acetic acid (DOTA(tBu)$_3$) or 2-(4,7,10-tris(2-(*tert*-butoxy)-2-oxoethyl)-1,4,7-triazacyclononane-1,4,7)-triacetic acid (NOTA(tBu)$_3$) to the peptide sequence LRELHLNNN via a polyethylene glycol link (PEG_2).

Fmoc-Asn(Trt)-OH (238.7 mg, 0.40 mmol) and diisopropylethylamine (DIEA) in 6.0 ml dry dichloromethane (DCM) was added to 2-chlorotrityl resin (375 mg, loading 1.6 mmol/g). After 2 h 0.30 ml MeOH was added and reacted for 15 min. The resin was washed with DMF (2 × 5 ml) and DCM (2 × 5 ml), dried in vacuum to give 584.5 mg. New loading was calculated to 0.64 mmol/g and the side chain protected peptide LRELHLNNN was synthesized in a 4 ml disposable syringe equipped with a porous polyethylene filter on a 374 μmol scale using SPPS and Fmoc/tert-butyl (tBu) protection. For the Fmoc protected amino acids the side chain protection was as follows: Asn(Trt), Arg(Pbf), Glu(Ot-Bu), His(Trt). 20% Piperidine in DMF (4 × 2 ml) was used to remove the Fmoc group after each coupling step and the amino acids was coupled overnight using PyBOP (540 μmol) in DMF (2 ml) in presence of DIEA (800 μmol). After completion of the coupling steps, the partially protected peptide on resin was washed with several portions of DMF, DCM and MeOH and dried in vacuum.

Part of the peptide on resin (approximately 30 μmol) was transferred to a 2 ml disposable syringe equipped with a porous polyethylene filter and after deprotection of the Fmoc-group coupled for 21 h with Fmoc-O2Oc-OH (Fmoc-PEG_2-OH, 2 equivalents) using PyBOP (2 equivalents) and DIEA (3 equivalents) in 0.5 ml DMF. The Fmoc group was removed by treatment with 20% piperidine in DMF (2 ml for 1 min + 3 × 2 ml for 10 min). After washing of the resin, DOTA(tBu)$_3$-OH (2 equivalents) or NOTA(tBu)$_3$-OH (2 equivalents) was coupled for 20 h using PyBOP, and DIEA DMF. The resin was then washed extensively with DMF and DCM and dried in vacuum.

The resin was transferred to a centrifuge tube and treated with triethylsilane (TES) followed of 95% aqueous TFA and the mixture was rotated for 2 h. The resin was removed by filtration and washed with TFA. The filtrate was partly evaporated under a stream of nitrogen and the peptide was precipitated by addition of diethyl ether. The precipitate was collected by centrifugation, washed with diethyl ether and dried in vacuum.

The crude peptides were dissolved in 10% acetonitrile in water and purified with preparative reversed high-preformance liquid chromatography (RP-HPLC). The preparative column used was a Nucleodur C18 HTec (21 × 125 mm, particle size 5 μm) and eluent was a MeCN/H_2O gradient with 0.1% TFA at a flow rate of 10 ml/min and with UV detection at 220 nm. The pure fractions were lyophilized and the two peptides was obtained with more than 98% purity determined from the 214 nm trace.

Analytical RP-HPLC was performed on a Dionex UltiMate 3000 HPLC system using a Penomenex Kinetex C18 column (50 × 3.0 mm, 2.6 μm particle size, 100 Å pore size). A gradient of H_2O/MeCN/0.05% HCOOH was used as at a flow rate of 1.5 ml/min. For detection UV and a Bruker amazon SL iontrap mass spectrometer with electrospray ionization (ESI) MS with positive mode scanning was used. The mass spectrometry analysis detected $m/z = 827.5$ for $[M + 2H]^{2+}$, 55.

1.8 for $[M + 3H]^{3+}$ and $m/z = 414.4$ for $[M + 4H]^{4+}$, with reconstituted molecular weight of 1652.85 for DOTA-PEG_2-LRELHLNNN and $m/z = 776.8$ for $[M + 2H]^{2+}$ and 518.3 for $[M + 3H]^{3+}$, with reconstituted molecular weight of 1551.8 for NOTA-PEG_2-LRELHLNNN.

2.3. Gallium-68 radiochemistry

A $^{68}Ge/^{68}Ga$ generator system with ^{68}Ge attached to a column packed with titanium dioxide (50 mCi, Cyclotron Co. Obninsk, Russia) was eluted with 0.1 M HCl, in order to obtain ^{68}Ga ($t_{½}$ = 68 min, β+ = 89% and EC = 11%). Second fraction of 1 ml containing 70–80% of the generator radioactivity was buffered with 100 μl of sodium acetate buffer (pH 7) to ensure pH 4.2–4.6. After controlling the pH, 20 nanomoles (1 mM, 600 μl) of DOTA-PEG_2-LRELHLNNN dissolved in deionized water was added, and the mixture with the total reaction volume of 1.7 ml was incubated in a heating block for 15 min at 75 °C. Following incubation, the crude product was left to cool down for 2 min and purified on solid phase extraction cartridge (HLB, Oasis) to obtain the pure product in 50% ethanol. Further, the product was analyzed on an HPLC-UV-Radio system (VWR Hitachi Chromaster pump 5110, Knauer UV detector 40D equipped with a remote UV flow cell, Bioscan Flow count equipped with an Eckert & Ziegler extended range module Model 106 and a Bioscan B-FC-3300 radioactivity probe and a VWR Hitachi Chromaster A/D Interface box). Separation of the analytes was accomplished using analytical column (Hichrom Vydac 214MS, 5 μm C4, 50 × 4.6 mm). The conditions were as followed: A = 0.1% TFA in H_2O; B = 0.1% TFA in 70% MeCN, with UV-detection at 220 nm; linear gradient over 15 min, 5–70% solvent B linear gradient over 15 min, flow rate was 1.0 ml/min. Data acquisition and handling were performed using Agilent OpenLAB Chromaster EZChrome Edition version A.04.05.

2.4. Aluminium fluoride-18 radiochemistry

Fluorine-18 was produced by a Scanditronix MC-17 cyclotron by proton bombardment of oxygen-18 enriched water (>97%). Typically, 3–5 GBq of radioactivity (at EOB) was produced. The radioactivity was transferred to a hotcell and passed through a QMA SPE cartridge to retain fluorine-18. The cartridge was washed with water (1 ml) and then the radioactivity was eluted with 200 μl NaCl solution (0.9%). To a 1.5 mL vial was added 20 μl NOTA-PEG_2-LRELHLNNN (40 nmol, 2 mM solution in NaOAc pH 4.6), 10 μl of $AlCl_3$ (2 mM in NaOAc pH 4.6), 50 μl NaOAc (pH 4.6) and 100 μl EtOH (99%). 50 μl of the saline solution containing fluorine-18 was added to a vial and then it was heated to 100 °C for 15 min. The reaction mixture was diluted with water (3 ml) and added to an HLB SPE cartridge which was then washed with water (3 × 1 ml). The product was eluted with 400 μl of EtOH (99%) and further diluted with 3.6 mL PBS. Quality control was performed in the same manner as with the gallium-68-labelled peptide using a gradient of 10–90% MeCN in 50 mM AMF over 8 min using a Phenomenex LUNA C18 column (5 μm, 150 × 4.6 mm).

2.5. Carbon tetrachloride induced liver fibrosis in mice

The most promising tracer analogue based on the biodistribution in liver was evaluated for in vitro and in vivo binding in a mouse model of hepatic fibrosis. Long-term exposure to carbon tetrachloride (CCl_4) is highly hepatotoxic due to lowered membrane permeability in the hepatic cellular compartments, which in the end will lead to reduced hepatic function, inflammation and induced fibrogenesis [15]. BALB/c mice (n = 6, female, 20 ± 1 g) received intraperitoneal injections in lower side of the abdomen of CCl_4 diluted in corn oil (20% CCl_4 solution, 0.5 mg/g) body weight three times/week for three weeks. The mice were monitored closely for 30 min after the CCl_4 injection and once per day, thereafter, to ensure their wellbeing. No animal reached the humane endpoint.

2.6. In vitro binding assay

Frozen mouse liver samples with various grade of fibrosis (from a CCl_4 model) as well as control livers, were sectioned to 20 μm sections

with a cryostat microtome (Micron HM560, Germany), mounted on Menzel Super Frost plus glass slides, dried at room temperature (RT) and stored at −20 °C until used in the study. The sections were pre-incubated for 10 min at RT in PBS buffer containing 1% BSA (to reduce tracer binding to the glass surface). Further, the sections were incubated at 200 nM (approximately at the expected K_d of 170 nM) concentration of [^{68}Ga]Ga-DOTA-PEG$_2$-LRELHLNNN for 40 min at RT in order to determine the total binding of the tracer. To determine the unspecific binding of the tracer, section duplicates were incubated in the presence of 60 μM unconjugated peptide, i.e. LRELHLNNN. Following the incubation with the tracer, the sections were washed 1 min in ice-cold PBS containing 1% BSA, and two times, 1 min each in ice-cold PBS. Further, the sections were dried under a stream of warm air (37 °C) for 10 min. As a reference, 20 μl of the incubation solution was applied to a filter paper. The sections together with the reference were exposed to phosphorimaging plates for 2.5 h, and scanned by a Phosphorimager system (Amersham Typhoon IP, GE Health). The sections were visualised and analyzed using the software ImageJ (ImageJ 1.45S, NIH, Bethesda, USA). Regions of interest (ROIs) were drawn on the liver tissues in the image, and the mean values of the tissue ROIs were corrected for background uptake. Specific binding was defined as the difference between total binding and non-displaceable binding, and the percentage of specific binding was defined as the ratio between the specific binding and the total binding multiplied by 100.

Separate sections from the same biopsy were stained with Sirius Red to assess the grade of fibrosis.

2.7. Organ distribution and dosimetry in healthy rats

Sprague Dawley rats, ($n = 22$, male, healthy, weight 287 ± 25 g) were used for ex vivo organ distribution assessment of biodistribution, dosimetry and in vivo stability (see Suppl. materials).

An activity of 3.3 ± 0.6 MBq of [^{68}Ga]Ga-DOTA-PEG$_2$-LRELHLNNN ($n = 10$) (corresponding to 8.3 μg) or 4.2 ± 1 MBq of [^{18}F]AlF-NOTA-PEG$_2$-LRELHLNNN ($n = 12$) (corresponding to 2 μg) in phosphate-buffered saline (PBS, pH 7.4) diluted with 0.9% NaCl, was injected intravenously as a bolus to conscious animals. The animals were euthanized by a CO_2–O_2 mixture 10, 20, 40, 60, 120 and 180 (fluorine-18 only) min post-injection. The radioactivity of the excised organs was measured in an automated gamma counter (2480 Wizard2™, PerkinElmer). Samples from blood, heart, lung, liver, spleen, adrenal glands, kidneys, intestines, with or without contents, muscle, testis, bone, brain, pancreas, urine bladder and bone marrow were collected. The remaining carcass was also measured in order to monitor the radioactivity elimination and recovery. The radioactivity readings were decay-corrected to the time of the injection, and the results were expressed as standardized uptake values (SUV) (Eq. (1)).

$$SUV\left(\frac{1}{1}\right) = \frac{Radioactivity_{tissue}(Bq) \Big/ Volume_{tissue}(cc)}{Radioactivity_{injected}(Bq) \Big/ Weight_{body}(g)} \quad (1)$$

Data from dynamic biodistribution data over 120 min time point on healthy rats was used to calculate the human predicted dosimetry. The residence times were calculated using trapezoidal model approximation of the organ uptake values (un-decay corrected) extrapolated to a model of human tissues weights. For dose assessment, OLINDA/EXM 1.1 software was used to compute the absorbed human doses in various organs on male phantoms.

Additionally, biodistribution was confirmed by PET/MRI imaging in additional rats using a small animal PET-MRI system (nanoPET/MRI, 3T, Mediso, Hungary). Anesthetized animals were administered 5 MBq [^{68}Ga]Ga-DOTA-PEG$_2$-LRELHLNNN ($n = 5$) or 10 MBq [^{18}F]AlF-NOTA-PEG$_2$-LRELHLNNN ($n = 3$) via the tail vein. Dynamic whole-body PET scanning for up to 150 min was performed using multiple whole-body sweeps (3 beds per pass; 2 × 5 min, 2 × 10 min, 4 × 30 min). Anatomical axial and coronal MR imaging were measured with T1-weighted (T1W) spin echo sequences. PET images were reconstructed by the use of Maximum Likelihood Estimation Maximized (MLEM) algorithm (10 iterations). Maximum Intensity Projection (MIP) images were generated in Carimas 2.9 (Turku PET Center, Turku, Finland) to allow quantitative visualization of radiotracer uptake distribution in the entire body.

2.8. Organ distribution and binding in mice with liver fibrosis

BALB/c mice treated with CCl_4 ($n = 6$) were used for biodistribution and binding experiments. Untreated BALB/c mice (n = 6) were used as controls. Four of the mice in each group were used for ex vivo organ distribution and autoradiography studies and $n = 2$ in each group for PET imaging.

An activity of 3 ± 0.4 MBq [^{68}Ga]Ga-DOTA-PEG$_2$-LRELHLNNN diluted with 0.9% NaCl, was injected intravenously to the treated and untreated mice ($n = 12$). After 60 min, four animals from each group were euthanized and the radioactivity of the excised organs was measured in a gamma counter, as described for rats above. In vivo stability of the tracer in blood was assessed in the control mice (see Suppl. Fig. S2).

Two animals from each group were examined by whole-body PET/MRI. Dynamic PET images were acquired from injection to 60 min and reconstructed as described above for the rats. After the PET acquisition, the animals were euthanized by sodium thiopental (Apoteket AB, Stockholm, Sweden) while lying in the scanner. PET images were analyzed in PMOD 4.0 (PMOD Technologies, Zürich, Switzerland) and MRI images in Nucline (Mediso, Hungary).

The liver from all animals was divided into three parts; one was used for the gamma counter reading as described above. The second was snap frozen, embedded in OCT media, processed into 10 μm sections and exposed to a phosphorimager plate with a known reference for quantification (i.e. ex vivo autoradiography). The third part was fixed in formalin and stained for collagen with Sirius Red.

2.9. In vitro plasma stability of [^{68}Ga]Ga-DOTA-PEG$_2$-LRELHLNNN

Plasma was harvested from an anesthetized male Sprague Dawley rat ($n = 1$) via heart puncture to a heparinized tube (BD Vaccutainer®). The plasma was separated from red blood cells by centrifugation at 4 °C and 3900 RCF (Beckman Coulter, Allegra™ X-22R). [^{68}Ga]Ga-DOTA-PEG$_2$-LRELHLNNN formulated in 50% ethanol (50 μl, approx. 25 MBq, approx. 1 nmol peptide) was added to rat plasma (450 μl, pre-heated to 37 °C, in a 1.5 ml Eppendorf tube). The mixture was vortexed for 15 s and then incubated in a heated vial shaker at 37 °C (Eppendorf Mixmate). HPLC samples (10 μl) were withdrawn at the following time points (1, 15, 30, 45 and 90 min) and injected directly to the HPLC without any further workup. Radioactivity recovery from the HPLC system was determined to 85% by comparing the radioactivity of a 10 μl reference sample with a sample of collected eluent from the column outlet from a 10 μl HPLC injection, using a well counter (built in house). A monolith Phenomenex Onyx C18 4.6 × 10.0 mm HPLC column was used for chromatography. Flowrate was 1.0 ml·min^{-1} during the analysis (0–9 min) and 2.5 ml·min^{-1} during wash (9–12 min). Solvents were A: 0.1% TFA in H_2O, B: 0.1% TFA in acetonitrile. A solvent gradient ranging from 10%B to 90%B over 9 min was applied and then the system was rinsed and re-equilibrated. t_R free $^{68}Ga^{3+}$: 1.65 min, t_R unidentified peptide fragments: 3.96, 4.90 and 5.36 min, t_R intact [^{68}Ga]Ga-DOTA-PEG$_2$-LRELHLNNN: 5.81 min.

2.10. In vivo stability analysis of [^{68}Ga]Ga-DOTA-PEG$_2$-LRELHLNNN

In vivo stability of [^{68}Ga]Ga-DOTA-PEG$_2$-LRELHLNNN was evaluated in healthy rat ($n = 1$, time points 5, 30 and 60 min after injection) and control mice ($n = 5$, 60 min post injection). Blood samples were taken at the indicated time points post injection into an EDTA-treated plastic

vial (to supress coagulation). The vial was kept on ice (to supress further metabolism) until centrifuged at 4 °C (10,000 rpm) to separate plasma. A 2 ul (or 5 ul for mouse 4, 5 and 6) plasma sample was added to the baseline of the iTCL strip and then eluted in a solution of 0.1 M EDTA in NH_4OAc 0.25 M pH 5.5. The strips were placed on a phosphorimager plate for 4 h. The plate was then scanned on a PerkinElmer Cyclone apparatus (600 dpi resolution) and the resulting images were analyzed using the instrument software. Control iTCL experiments were performed to confirm the R_f values of the intact tracer [^{68}Ga]Ga-DOTA-PEG_2-LRELHLNNN (from QC sample, stays at baseline) as well as $^{68}Ga^{3+}$ in 0.1 M HCl (direct from generator, goes with solvent front).

3. Results

3.1. Radiolabelling

DOTA-PEG_2-LRELHLNNN was labelled with ^{68}Ga ($n = 7$) and purified using a solid-phase extraction cartridge, resulting in a radiochemical purity of >97% (Fig. 1B and Suppl. Fig. S1A). The activity yield was 88–90 MBq (non-decay corrected).

NOTA-PEG_2-LRELHLNNN was labelled with Al^{18}F ($n = 5$) and purified using a solid-phase extraction cartridge, resulting in a radiochemical purity of >99% (Fig. 1C and Suppl. Fig. S1B). The activity yield was 0.3–0.8 GBq (10–20%, non-decay corrected).

3.2. In vitro binding assay

In vitro autoradiography experiments were performed in order to assess the correlation of tracer binding in liver sections with the grade of fibrosis. [^{68}Ga]Ga-DOTA-PEG_2-LRELHLNNN demonstrated a significant correlation ($p < 0.05$) in binding (in the range of 1–80 fmol/mm^3) to grade 0–3 fibrotic liver tissue ($n = 10$), with a correlation coefficient of 0.4 (Fig. 2A).The uptake of 200 nM [^{68}Ga]Ga-DOTA-PEG_2-LRELHLNNN by the frozen sections of fibrotic mice liver was inhibited using 60 μM of unconjugated LRELHLNNN peptide (Fig. 2B). No detectable blocking effect was observed in healthy controls without fibrosis, as expected. The binding to healthy liver tissue controls ($n = 2$) was in the range of 2–22 fmol/mm^3. Representative Sirius red staining for collagen in mild and severe fibrotic liver tissues are shown (Fig. 2C-D).

3.3. Organ distribution and dosimetry in healthy rats

Ex vivo organ distribution data from 19 organs is presented as decay-corrected SUV values. [^{68}Ga]Ga-DOTA-PEG_2-LRELHLNNN revealed fast blood clearance and washout from most of the organs with SUV values below one (Fig. 3A). The kidney SUV was at the level of four at the 10 min time point, with a decrease to SUV ≈ 1 after 120 min p.i., indicating on fast renal excretion and low renal trapping. The pattern of the biodistribution was the same as assessed by dynamic PET ($n = 3$) (Fig. 3B). The total effective dose for [^{68}Ga]Ga-DOTA-PEG_2-LRELHLNNN was 13 μSv/MBq. The effective dose allows administration of up to 770 MBq to humans annually; corresponding to at least three PET scans of 200 MBq.

For the [^{18}F]AlF-NOTA-PEG_2-LRELHLNNN tracer, the organ distribution profile demonstrated SUV values above one for most organs at early time points (Fig. 3C). Blood SUV value was on the level of three at 10 min p.i and decreased to one at 60 min p.i and further to 0.1 at 180 min p.i. Liver revealed an increasing uptake until 40 min p.i reaching SUV value of 5, followed by a decrease at 180 min with a SUV value below one. Kidney uptake was elevated throughout all timepoints. Again, the biodistribution for [^{18}F]AlF-NOTA-PEG_2-LRELHLNNN was verified by PET imaging (Fig. 3D). The total effective dose for [^{18}F]AlF-NOTA-PEG_2-LRELHLNNN was 15.4 mSv/MBq which allows for administration of 649 MBq.

3.4. Organ distribution and binding in mice with liver fibrosis

[^{68}Ga]Ga-DOTA-PEG_2-LRELHLNNN was evaluated for in vivo targeting of collagen type I in a mouse model of liver fibrosis. Organ resection and measurement after 60 min post injection demonstrated low

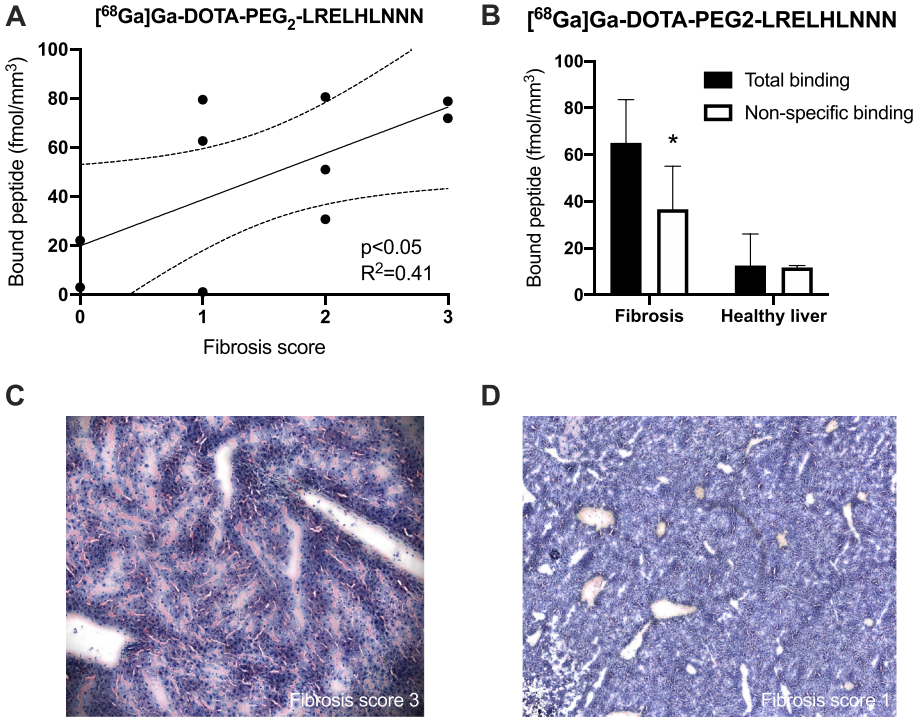

Fig. 2. In vitro autoradiography of radiolabelled LRELHLNNN towards liver fibrosis sections. [^{68}Ga]Ga-DOTA-PEG_2-LRELHLNNN demonstrated binding to increasing grades of fibrosis (A) as well as partly blockable binding in all fibrotic sections with uptake above background (B). Severe fibrosis and mild fibrosis, stained by Sirius Red, are represented by figures C and D, respectively.

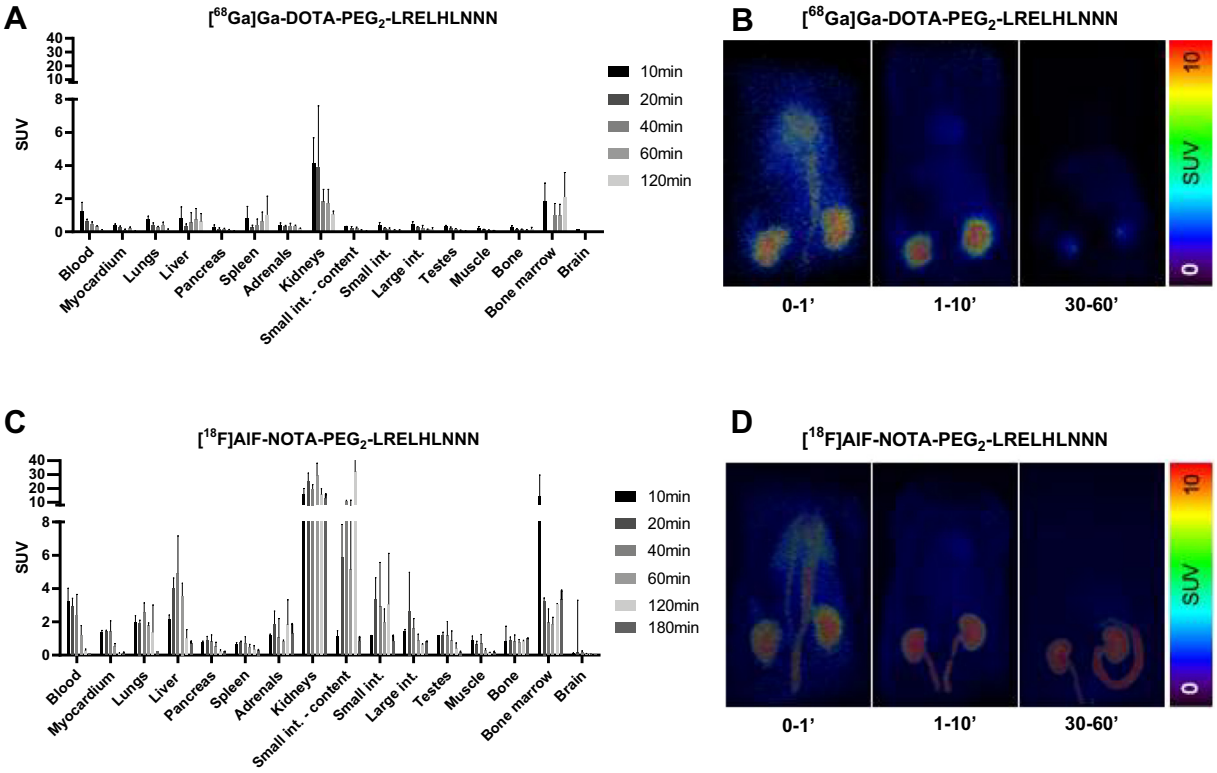

Fig. 3. In vivo biodistribution and nanoPET/MRI images of [^{68}Ga]Ga-DOTA-PEG$_2$-LRELHLNNN (A-B) and [^{18}F]AlF-NOTA-PEG$_2$-LRELHLNNN (C-D) in healthy Sprague Dawley rats.

uptake in most tissues, similar to healthy rats. The SUV values for the tracer were below one for all organs. Kidneys had the highest SUV at the level of 0.8. The uptake in fibrotic liver was in the range of SUV ≈ 0.3, which is low in absolute magnitude but still higher than all other tissues except kidney (Fig. 4A). However, also the control mice exhibited a similar hepatic uptake on a whole organ level (not significant). The ex vivo autoradiograms revealed a consistent heterogeneity and higher uptake of [^{68}Ga]Ga-DOTA-PEG$_2$-LRELHLNNN in distinct parts of the liver in all mice with induced fibrosis (Fig. 4B).

3.5. Plasma and in vivo stability analysis of [^{68}Ga]Ga-DOTA-PEG$_2$-LRELHLNNN

[^{68}Ga]Ga-DOTA-PEG$_2$-LRELHLNNN stability was assessed both in plasma in vitro (rat) and in vivo (rat and mouse). In plasma, up to 75% of [^{68}Ga]Ga-DOTA-PEG$_2$-LRELHLNNN was intact after 90 min (Fig. 5A). Of the metabolites at this time-point, around 10% consisted of free $^{68}Ga^{3+}$ and the rest ^{68}Ga-peptide fragments.

In vivo, appearance of radiolabeled metabolites in plasma after injection were demonstrated both in rats and mice (Fig. 5B). Only 10–15% of radioactivity corresponded to intact [^{68}Ga]Ga-DOTA-PEG$_2$-LRELHLNNN after 60 min. In rat, the main metabolites were ^{68}Ga-peptide fragments (approximately 75%) while the rest corresponded to free $^{68}Ga^{3+}$ (approximately 15%).

4. Discussion

Here, we demonstrate robust radiolabelling of chelator conjugated high affinity peptides for targeting of collagen type I, as well as their preclinical evaluation.

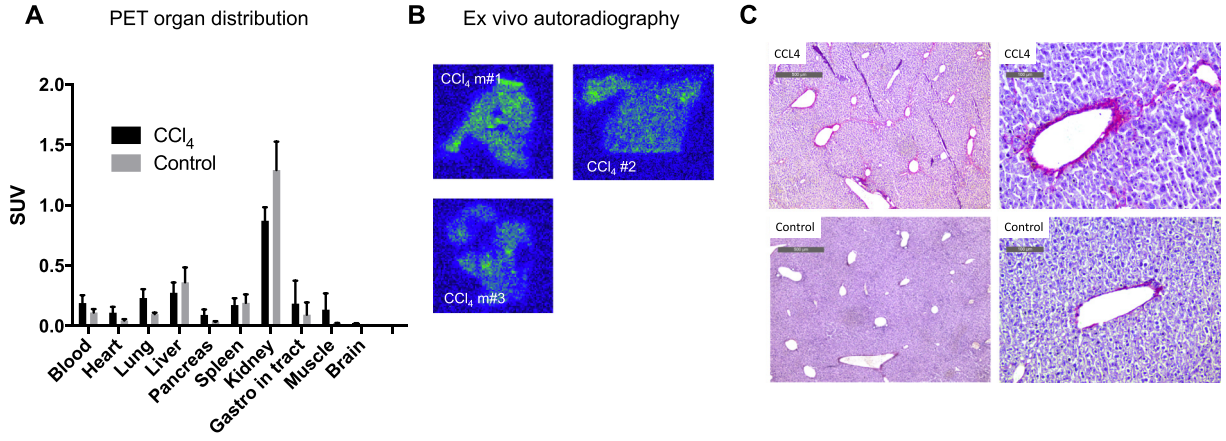

Fig. 4. Organ distribution of [^{68}Ga]Ga-DOTA-PEG$_2$-LRELHLNNN in a mouse model of induced liver fibrosis compared to control mice (A). Ex vivo autoradiograms consistently demonstrated heterogeneous patterns of [^{68}Ga]Ga-DOTA-PEG$_2$-LRELHLNNN binding in the fibrotic liver (B). Sirius Red staining of liver from CCl_4 treated and control mice, where collagen is seen in red/purple colour (C).

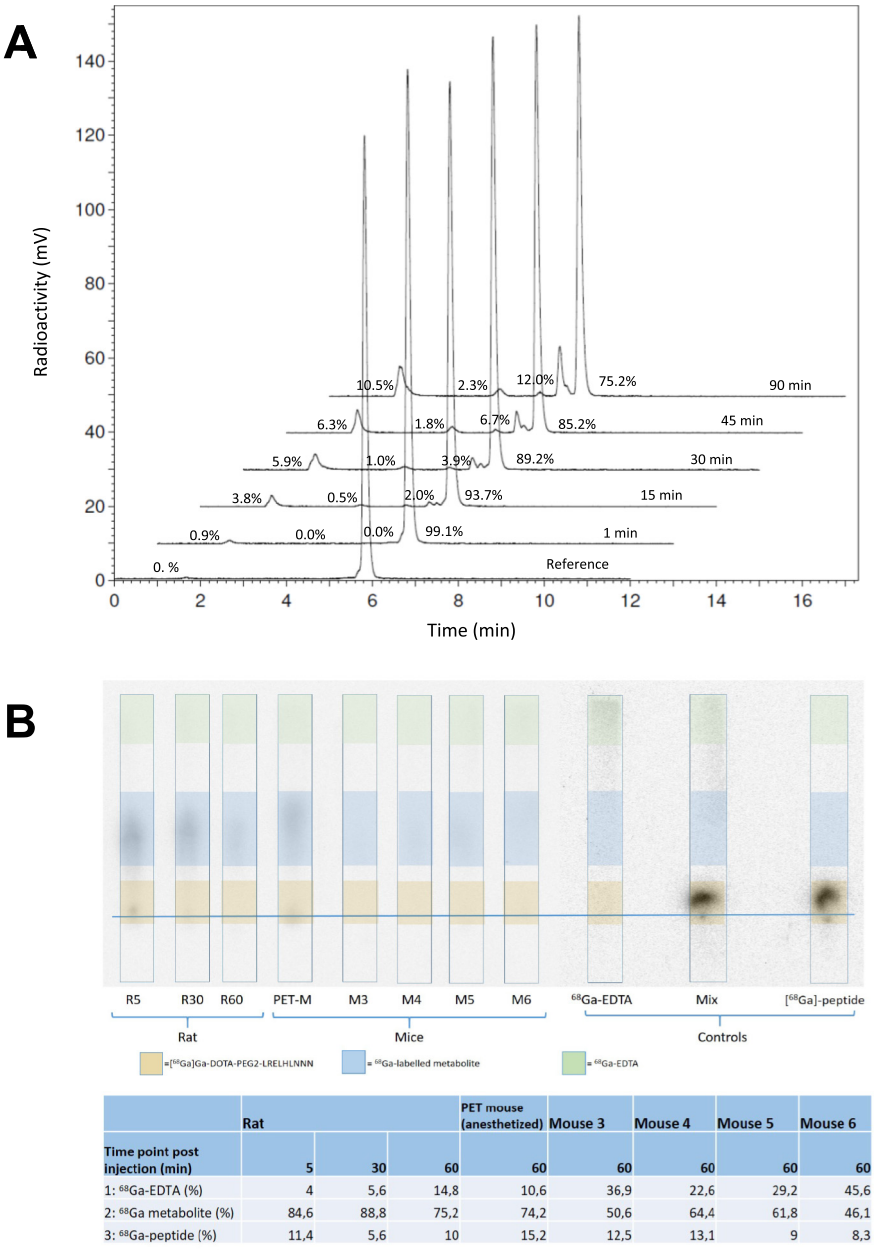

	Rat			PET mouse (anesthetized)	Mouse 3	Mouse 4	Mouse 5	Mouse 6
Time point post injection (min)	5	30	60	60	60	60	60	60
1: ^{68}Ga-EDTA (%)	4	5,6	14,8	10,6	36,9	22,6	29,2	45,6
2: ^{68}Ga metabolite (%)	84,6	88,8	75,2	74,2	50,6	64,4	61,8	46,1
3: ^{68}Ga-peptide (%)	11,4	5,6	10	15,2	12,5	13,1	9	8,3

Fig. 5. HPLC radiochromatograms from in vitro metabolic stability test of [^{68}Ga]Ga-DOTA-PEG$_2$-LRELHLNNN in rat plasma at 37 °C (A). In vivo stability of [^{68}Ga]Ga-DOTA-PEG$_2$-LRELHLNNN in plasma after injection in rat or mouse (B).

Clinical imaging techniques, such as computed tomography (CT) and MRI may already detect fibrosis lesions in the lungs and liver [16,17], however, it lacks sensitivity of detecting fibrosis on an early stage or small changes induced by interventions.

Several collagen binding monoclonal antibodies and endogenous proteins have been described [5], but these are generally unsuitable for imaging given the long circulating time in plasma thus requiring a long half-life radionuclide with corresponding high radiation dose to the subject. In comparison, the LRELHLNNN peptide consisting of just 9 amino acid residues is expected to exhibit rapid biodistribution and excretion, consistent with radiolabelling using short-lived positron emitting radionuclides.

The feasibility of in vivo imaging of fibrosis via targeting of collagen type I was recently demonstrated especially in lung, using two conceptually different radiolabelled peptides CBP8 [4,7–9] and collagelin [10–14], both with an affinity for collagen type I above micromolar range. Collagelin additionally targets collagen type III. Despite these promising results, both CBP8 and collagelin exhibits a relatively poor affinity for collagen, in the range of 1.5–2 μM. Normally, successful PET imaging requires an affinity in the nanomolar range, illustrated by the binding potential (BP) (Eq. (2)). To image a given target population, the B_{max} should be high and the K_d small (i.e. high affinity).

$$BP = \frac{B_{max}\ (\text{receptor density})}{K_d\ (\text{affinity})} \tag{2}$$

The success of the previously mentioned peptides is probably explained by the high amount of binding sites (high B_{max}) in fibrotic lesions, which yields an acceptable BP despite the low affinity (high K_d). Thus, with further improvements in K_d, such as the 10-fold increase in affinity seen for LRELHLNNN, we can expect to visualize a 10-fold lower fibrosis density. This is especially important for assessing small changes in collagen depositions, i.e. early in the development of

NAFLD/NASH or when assessing effects of intervention designed to decrease the fibrotic load in tissue.

[^{68}Ga]Ga-DOTA-PEG$_2$-LRELHLNNN demonstrated higher binding to liver sections with fibrosis compared to healthy tissues, consistent with the selectivity and affinity of the peptide for collagen type I. Importantly, the binding correlated to the grade of fibrosis as assessed by Sirius Red staining of collagen. However, there was overlap in tracer binding between the different grading of fibrosis, indicating limitations of sensitivity.

The biodistribution of [^{68}Ga]Ga-DOTA-PEG$_2$-LRELHLNNN and [^{18}F]AlF-NOTA-PEG$_2$-LRELHLNNN in healthy control animals was favorable. Both variants were assessed by ex vivo organ distribution and PET imaging. There was rapid clearance and low background binding in tissues where fibrosis may develop in the clinical situation, such as heart, liver, lung and brain. [^{18}F]AlF-NOTA-PEG$_2$-LRELHLNNN demonstrated generally higher retention in many tissues as evident from ex vivo gamma counter analysis (Fig. 3B). The biodistribution of [^{18}F]AlF-NOTA-PEG$_2$-LRELHLNNN was independently demonstrated by the PET imaging analysis, confirming stronger background in most tissues, and retention in both kidney and small intestine (Fig. 3B).

Due to differences in molar activity, less peptide mass of [^{18}F]AlF-NOTA-PEG$_2$-LRELHLNNN (2 μg) was injected compared to [^{68}Ga]Ga-DOTA-PEG$_2$-LRELHLNNN (≈8 μg). However, it would be surprising if the difference in biodistribution should be due to a peptide mass effect at such low mass doses. Furthermore, the in vivo stability was evaluated for [^{68}Ga]Ga-DOTA-PEG$_2$-LRELHLNNN but not for [^{18}F]AlF-NOTA-PEG$_2$-LRELHLNNN. Thus, the stability of the respective peptide may differ, although unlikely, and thereby affect the biodistribution.

Importantly, [^{68}Ga]Ga-DOTA-PEG$_2$-LRELHLNNN demonstrated rapid clearance also from kidney. Fibrosis development in kidney is a complication from e.g. metabolic disease, but visualization of the kidney is a general problem in PET since many peptides and small molecules demonstrate strong retention in this tissue [18]. [^{68}Ga]Ga-DOTA-PEG$_2$-LRELHLNNN exhibited an uptake of less than SUV < 2 after 60 min, potentially enabling collagen type I imaging also in kidney. Previous collagen type I PET tracers demonstrated much higher renal retention in kidney (^{68}Ga-DOTA-CBP8: SUV ≈ 10 and ^{68}Ga-NO2A-Collagelin: SUV > 6, both 60 min after administration [4,12]), presumably due to partial re-uptake and trapping of the radionuclide in the renal cortex. Thus, the DOTA-PEG$_2$-LRELHLNNN scaffold for the first time provide a plausible alternative for imaging of renal fibrosis. [^{18}F]AlF-NOTA-PEG$_2$-LRELHLNNN biodistribution generally exhibited a somewhat higher background binding in most tissues, especially kidney and liver. On the other hand, there was no incorporation of fluorine-18 in bone, indicating stability of the radiolabel.

An adequate fibrosis monitoring during diagnosis as well as in the drug development setting would potentially require repeated imaging assessments. It is therefore of great importance to demonstrate that the intended tracer does not affect radiosensitive organs, such as the bone marrow. The extrapolated human predicted dosimetric profiles of both [^{68}Ga]Ga-DOTA-PEG$_2$-LRELHLNNN and [^{18}F]AlF-NOTA-PEG$_2$-LRELHLNNN were beneficial, potentially allowing several PET examinations annually also in relatively healthy individuals while still adhering to the safety limits for Category IIb effective dose regarding radiation exposure (10 mSv) in adults (e.g. the relevant category for examinations "aimed directly at the diagnosis, cure or prevention of disease") [19].

Based on the lower background binding in liver, [^{68}Ga]Ga-DOTA-PEG$_2$-LRELHLNNN was further evaluated in a mouse model of liver fibrosis. [^{68}Ga]Ga-DOTA-PEG$_2$-LRELHLNNN binding to fibrotic liver was higher that surrounding tissues, approximately 2 times higher than in blood and spleen. However, the absolute magnitude of binding, in the range of SUV 0.3 was low, indicating limited targeting of the tracer to liver. This was further confirmed by the observation of a similar hepatic binding of [^{68}Ga]Ga-DOTA-PEG$_2$-LRELHLNNN in healthy control.

This state-of-the-affairs is likely due to two main reasons: firstly 3 weeks of CCl_4 treatment is a relatively mild model of fibrosis (Fig. 4B). Stronger grade of fibrosis may be generated by 6 weeks of treatment [15], sometimes in combination with other adjunct treatments such as high fat diet. The sensitivity of [^{68}Ga]Ga-DOTA-PEG$_2$-LRELHLNNN may be too low for detecting the relative low amounts of hepatic fibrosis induced by 3 weeks of treatment. Secondly, the LRELHLNNN peptide was relatively stable in plasma in vitro, but not in vivo. Partial degradation would explain the limited binding seen in the in vivo mouse model. The identity of the metabolites appearing in the stability analysis in rat and mouse plasma was not further investigated, but is likely peptide fragments still incorporating DOTA chelated Gallium-68. This metabolic instability is not entirely surprising as its design has not incorporated consideration for in vivo proteolytic stability e.g. C-terminal is unprotected, all residues are L-amino acids etc. [5,6]. Optimization of this peptide scaffold may even further improve the sensitivity for PET imaging of Collagen type 1 deposits.

5. Conclusion

We describe the modification, radiolabelling and evaluation of the collagen type I binding peptide LRELHLNNN. The resulting radiotracer analogues demonstrated suitable biodistribution and dosimetry. [^{68}Ga]Ga-DOTA-PEG$_2$-LRELHLNNN in particular exhibited in vitro binding to hepatic fibrotic lesions, as well as low in vivo background uptake in normal tissue. Although [^{68}Ga]Ga-DOTA-PEG$_2$-LRELHLNNN could serve as a promising tool for PET imaging of fibrosis, improved proteolytic stability is required for further progress.

Supplementary data to this article can be found online at https://doi.org/10.1016/j.nucmedbio.2020.11.006.

Declaration of competing interest

Olof Eriksson and Christer Westerlund are employees of Antaros Medical AB. Otherwise, the authors have nothing to disclose.

Acknowledgements

The study was funded by Magnus Bergvall's Foundation and Science for Life Laboratory. We thank the Preclinical PET/MRI Platform for their support during the conduct and analysis of this study. We thank Suha Sarhan for assistance in synthesis of peptide precursors.

References

[1] Distler JHW, Györfi AH, Ramanujam M, Whitfield ML, Königshoff M, Lafyatis R. Shared and distinct mechanisms of fibrosis. Nat Rev Rheumatol. 2019;15(12):705–30 Dec.
[2] Altamirano-Barrera A, Barranco-Fragoso B, Méndez-Sánchez N. Management strategies for liver fibrosis. Ann Hepatol. 2017;16(1):48–56 Jan-Feb.
[3] Aydın MM, Akçalı KC. Liver fibrosis. Turk J Gastroenterol. 2018;29(1):14–21 Jan.
[4] Désogère P, Tapias LF, Hariri LP, Rotile NJ, Rietz TA, Probst CK, et al. Type I collagen-targeted PET probe for pulmonary fibrosis detection and staging in preclinical models. Sci Transl Med. 2017;9(384) Apr 5.
[5] Federico S, Pierce BF, Piluso S, Wischke C, Lendlein A, Neffe AT. Design of decorin-based peptides that Bind to collagen I and their potential as adhesion moieties in biomaterials. Angew Chem Int Ed Engl. 2015;54(37):10980–4 Sep 7.
[6] Wahyudi H, Reynolds AA, Li Y, Owen SC, Yu SM. Targeting collagen for diagnostic imaging and therapeutic delivery. J Control Release. 2016;240:323–31 Oct 28.
[7] Polasek M, Fuchs BC, Uppal R, Schühle DT, Alford JK, Loving GS, et al. Molecular MR imaging of liver fibrosis: a feasibility study using rat and mouse models. J Hepatol. 2012;57(3):549–55 Sep.
[8] Désogère P, Tapias LF, Rietz TA, Rotile N, Blasi F, Day H, et al. Optimization of a collagen-targeted PET probe for molecular imaging of pulmonary fibrosis. J Nucl Med. 2017;58(12):1991–6 Dec.
[9] Montesi S, Izquierdo-Garcia D, Abston E, Desogere P, Seethamraju R, Lanuti M, et al. Collagen-targeted PET imaging in pulmonary fibrosis: initial human experience. J Nucl Med. 2019;60(supplement 1):297 May 1.
[10] Muzard J, Sarda-Mantel L, Loyau S, Meulemans A, Louedec L, Bantsimba-Malanda C, et al. Non-invasive molecular imaging of fibrosis using a collagen-targeted peptidomimetic of the platelet collagen receptor glycoprotein VI. PLoS One. 2009;4(5):e5585.

[11] Chilakamarthi U, Kandhadi J, Gunda S, Thatipalli AR, Kumar Jerald M, Lingamallu G, et al. Synthesis and functional characterization of a fluorescent peptide probe for non invasive imaging of collagen in live tissues. Exp Cell Res. 2014;327(1):91–101 Sep 10.
[12] Velikyan I, Rosenström U, Estrada S, Ljungvall I, Häggström J, Eriksson O, et al. Synthesis and preclinical evaluation of 68Ga-labeled collagelin analogs for imaging and quantification of fibrosis. Nucl Med Biol. 2014;41(9):728–36 Oct.
[13] Velikyan I, Rosenström U, Bulenga TN, Eriksson O, Antoni G. Feasibility of multiple examinations using (68)Ga-labelled collagelin analogues: organ distribution in rat for extrapolation to human organ and whole-body radiation dosimetry. Pharmaceuticals (Basel). 2016 Jun 6;9(2).
[14] Kim H, Lee SJ, Kim JS, Davies-Venn C, Cho HJ, Won SJ, et al. Pharmacokinetics and microbiodistribution of 64Cu-labeled collagen-binding peptides in chronic myocardial infarction. Nucl Med Commun. 2016;37(12):1306–17 Dec.
[15] Scholten D, Trebicka J, Liedtke C, Weiskirchen R. The carbon tetrachloride model in mice. Lab Anim. 2015 Apr;49(1 Suppl):4–11.
[16] Annet L, Peeters F, Abarca-Quinones J, Leclercq I, Moulin P, Van Beers BE. Assessment of diffusion-weighted MR imaging in liver fibrosis. J Magn Reson Imaging. 2007;25(1):122–8 Jan.
[17] Petitclerc L, Gilbert G, Nguyen BN, An Tang. Liver fibrosis quantification by magnetic resonance imaging. Top Magn Reson Imaging. 2017;26(6):229–41 Dec.
[18] Gotthardt M, van Eerd-Vismale J, Oyen WJG, de Jong M, Zhang H, Rolleman E, et al. Indication for different mechanisms of kidney uptake of radiolabeled peptides. J Nucl Med. 2007;48(4):596–601 Apr.
[19] European Commission guidelines “Radiation protection 99, guidance on medical exposures in medical and biomedical research”. Directorate-general environment, nuclear safety and civil protection; 1998.